

**Observation of the symmetry of core states of a single Fe impurity in GaAs**J. Bocquel,<sup>1</sup> V. R. Kortan,<sup>2,3</sup> R. P. Campion,<sup>4</sup> B. L. Gallagher,<sup>4</sup> M. E. Flatté,<sup>1,2,3</sup> and P. M. Koenraad<sup>1</sup><sup>1</sup>*Department of Applied Physics, Eindhoven University of Technology, P.O. Box 513, 5600 MB, Eindhoven, The Netherlands*<sup>2</sup>*Department of Physics and Astronomy, University of Iowa, Iowa City, Iowa 52242, USA*<sup>3</sup>*Optical Science and Technology Center, University of Iowa, Iowa City, Iowa 52242, USA*<sup>4</sup>*School of Physics and Astronomy, University of Nottingham, Nottingham NG7 2RD, United Kingdom*

(Received 23 January 2015; published 23 August 2017)

We report the direct observation of two mid-gap core  $d$  states of differing symmetry for a single Fe atom embedded in GaAs. These states are distinguished by the strength of their hybridization with the surrounding host electronic structure. The midgap state of Fe that does not hybridize via  $\sigma$  bonding is strongly localized to the Fe atom, whereas the other, which does, is extended and comparable in size to other acceptor states. Tight-binding calculations of these midgap states agree with the spatial structure of the measured wave functions and illustrate that such measurements can determine the degree of hybridization via  $\pi$  bonding of impurity  $d$  states. These single-dopant midgap states with strong  $d$  character, which are intrinsically spin-orbit-entangled, provide an opportunity for probing and manipulating local magnetism and may be of use for high-speed electrical control of single spins.

DOI: [10.1103/PhysRevB.96.075207](https://doi.org/10.1103/PhysRevB.96.075207)**I. INTRODUCTION**

The electronic localization of single-dopant states within the electronic energy gap of a host semiconductor provides a model pseudoatomic system to manipulate in an effective semiconductor “vacuum” [1,2]. Recent progress in single-dopant measurement and manipulation has included optical and electronic addressing of individual spin centers [3,4], observation of virtual internal transitions among midgap states [5], valley-orbit coupling [6], and the effects of strain on the symmetry of the electronic wave functions [7,8]. An individual transition-metal dopant in a tetrahedrally bonded semiconductor can provide access to most of these phenomena [7,9,10]. In addition, the potential for very large impurity spin-orbit and exchange interactions has suggested new ways to probe [11] and manipulate local spins and magnetic properties using electric fields [9], strain [7], or a surface [12]. For a specific single substitutional transition-metal dopant in a tetrahedrally bonded semiconductor, the electronic structure of the midgap states is governed by charge-transfer energies,  $d$ -state filling, and the compatibility of  $d$ -orbital symmetry with the bonding in the surrounding host [13,14]. In the absence of spin-orbit splitting, the  $d$  states of a substitutional impurity split in the crystal field into two types of states with very different symmetry relative to the host: so-called  $e$  and  $t_2$  states. The  $t_2$  states have the same symmetry in the crystal field as the  $p$  orbitals, and hence hybridize efficiently with them along the  $\sigma$  bonds connecting the impurity to its four nearest neighbors [15]. The  $e$  states, in contrast, have an incompatible symmetry with the  $p$  orbitals via  $\sigma$  bonding [16], but could hybridize through the much weaker  $\pi$  bonding, or through  $\sigma$  bonding and spin-orbit mixing, to the four nearest neighbors. To date the acceptor features seen for acceptors in tetrahedrally bonded semiconductors [5,17–25] have all been associated with  $t_2$  symmetry, including Zn, Mn, Co, and Fe.

Here we report the direct observation with scanning tunneling microscopy (STM) and scanning tunneling spectroscopy (STS) of  $d$  states that have  $e$  symmetry and hybridize with the surroundings around a single subsurface Fe impurity

substituted for a Ga atom below the (110) surface of GaAs. The hybridization is very weak for these  $e$  states compared to the previously observed  $t_2$  states, which manifests in a much more localized apparent wave function for the  $e$  state than the simultaneously observed  $t_2$  state around the same Fe impurity. A theoretical description of the electronic states requires a technique that can describe the wave function on tens of thousands of atoms while preserving the local orbital symmetry in the basis; this description can be implemented in a tight-binding theory that describes the electronic structure of the host using an empirical basis [26–28] and matches the  $3d$  levels of the impurity from *ab initio* calculations, consistent with experimental measurements. With this approach, the theoretical calculations show excellent agreement with the spatial structure of the  $t_2$  states and, with very weak  $3d$ - $4p\pi$  hybridization between the Fe and the surrounding As atoms, provides excellent agreement for the spatial structure of the  $e$  states. The penetration of  $e$  states of an Fe impurity into the surrounding GaAs, even with very weak  $pd\pi$  hybridization, also suggests that the hybridization of rare-earth dopants with a surrounding tetrahedrally bonded host may be observable. Although our treatment here is applied to zincblende semiconductors, the analysis and expectations in terms of  $e$  and  $t_2$  states extends to solids with cubic point group symmetry ( $O_h$ ), which includes materials with diamond symmetry such as silicon and germanium, as well as other cubic crystals with a band gap.

The spatial structure of the  $t_2$  and  $e$  orbitals of a  $3d$  transition-metal atom in a tetrahedrally bonded semiconductor, as well as the symmetry of the orbital overlaps with  $p$  orbitals on the neighboring As atoms in the absence of spin-orbit interactions, are shown in Fig. 1(a). The electronic configuration of the free atom is  $[\text{Ar}] s^2 d^n$ , with  $n$  electrons in the  $d$  shell. In order to replace a cation with an  $s^2 p^1$  electronic configuration and act as an isoelectronic impurity in the host crystal, a transition-metal atom  $M$  should release three electrons, of which two are  $4s$  electrons and one is a  $3d$  electron. The electronic configuration becomes  $M^{3+} (d^{n-1})$  with  $n - 1$  electrons in the  $d$  shell. The  $3d$  shell is

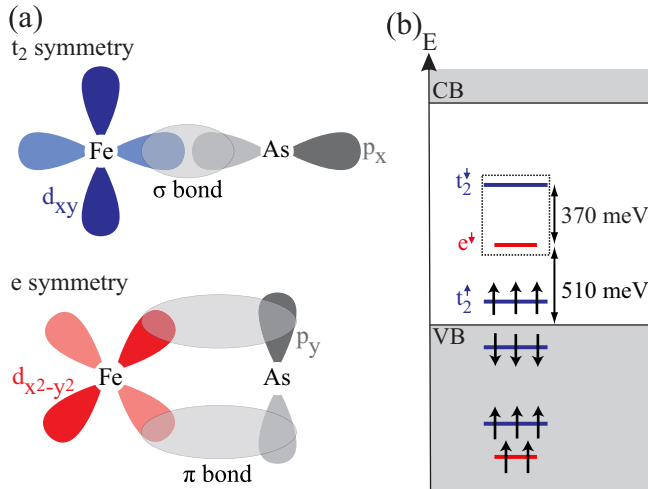


FIG. 1. (a)  $\sigma$  and  $\pi$  bonding of  $3d$  transition-metal atom to one of its nearest neighbors in a tetrahedrally bonded semiconductor along with the relative spatial orientation of the  $t_2$  and  $e$  orbitals. More lightly shaded orbital lobes have amplitudes of opposite sign to those of the darker shaded lobes. (b) Energy levels and occupation of the  $\text{Fe}^{3+}$  ion (with five  $d$  electrons) in GaAs semiconductor bands. The  $e$  impuritylike level plays an important role in the physics of charge transfer; its occupation, i.e., its position relative to the Fermi level, determines whether the Fe impurity is in its  $\text{Fe}^{3+}$  or  $\text{Fe}^{2+}$  state.  $e$  levels, midgap, and valence-band-resonant  $t_2$  levels are respectively indicated in red and blue. Arrows indicate the energy separation between the empty  $t_2$  and  $e$  midgap levels that will be imaged, and the height of the empty  $e$  level above the valence band. The  $t_2^\uparrow$  states are indicated above the valence maximum to clarify the energy required for placing a hole into the system on the same energy diagram as that required for adding an electron into the system.

partially filled and the  $4sp^3$  states form the outermost shell. Figure 1(b) shows the energies of the resulting features in the spectrum, with a dashed black frame around the  $t_2$  and  $e$  features investigated in this paper. The different transition energies shown in this diagram were determined by optical spectroscopy [29,30].

## II. STM MEASUREMENTS OF Fe IMPURITY STATES

These  $t_2$  and  $e$  states are observed in cross-sectional STM (X-STM) performed at 5 K under UHV conditions ( $5 \times 10^{-11}$  torr). Several electrochemically etched tungsten STM tips were used. The STM was operated in constant current mode on a clean and atomically flat GaAs (110) surface obtained by *in situ* cleavage. The molecular beam epitaxy grown sample contains a 100-nm Fe-doped GaAs layer (nominal concentration of  $2 \times 10^{18} \text{ cm}^{-3}$ ) and an Fe monolayer incorporated in GaAs. The growth temperature was  $480^\circ \text{C}$  during the entire growth procedure. The nominal layer structure consisted of GaAs substrate/100 nm Fe:GaAs/200 nm GaAs/Fe monolayer/500 nm GaAs. In order to improve the chance to locate Fe impurities in the structure both a bulk doped and a  $\delta$ -doped layer are included in the sample. The two Fe-doped regions are codoped with C atoms (nominal concentration of  $2 \times 10^{18} \text{ cm}^{-3}$ ). These shallow acceptors greatly increase the conductivity at the experiment's temperature of

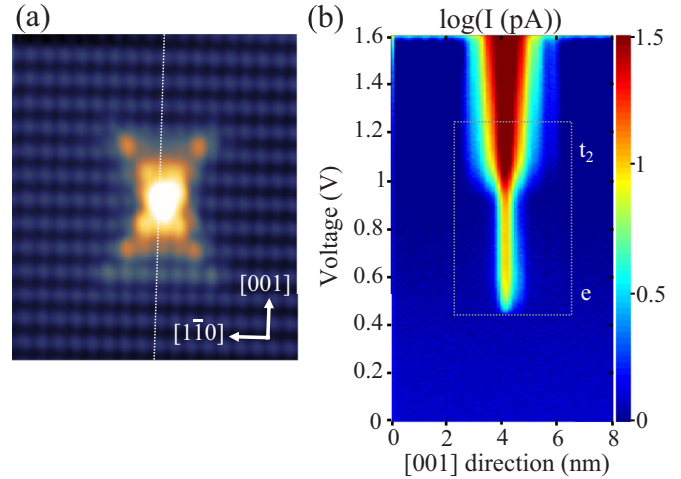


FIG. 2. (a)  $7.5 \times 7$ -nm empty-states image of a single Fe impurity. (b) The current cross section taken across the Fe impurity along the [001] direction. The current data taken directly on the Fe center show two distinct onsets around  $+0.45 \text{ V}$  and  $+1.0 \text{ V}$ , which are attributed to two states related to Fe. The onset of the conduction band is visible at a voltage of  $1.55 \text{ V}$ .

5 K, while having little influence on the position of the sample Fermi level (which is in the gap, close to the top of the valence band). The C impurities are clearly distinguishable from the Fe impurities due to their very different contrast; the C-related features show up with a more extended triangular shape [31], as opposed to the more bow-tie-shaped contrast of the Fe-related features (see Supplemental Material [32]).

The empty-states topography image of single subsurface Fe impurity shown in Fig. 2(a) presents a bright and anisotropic contrast. This feature shows a strong similarity with the contrast reported for the subsurface  $[\text{Mn}^{2+} + \text{h}^+]$  neutral acceptor state [20]. Both contrasts share common features like their brightness and their anisotropic shape. The anisotropic shape, clearly visible at low voltages, fades away at higher voltages as reported for other acceptors [20]. This evolution is not completely gradual. Above  $V = +1.7 \text{ V}$ , the anisotropic shape disappears for the most part, leaving only a bright localized contrast, while a clear change in corrugation of the GaAs surface is observed. This is explained by the contribution of empty conduction band states above  $V = +1.7 \text{ V}$ , which overwhelms the smaller local density of states of the midgap states.

The bright electronic contrast of the Fe atom is perfectly symmetric with respect to the [001] axis and highly symmetric with respect to the  $[1\bar{1}0]$  axis. In the case of Mn atoms in GaAs, it has been shown that the degree of asymmetry with respect to the  $[1\bar{1}0]$  axis is related to the interaction between the Mn state with the asymmetric buckled surface [33], and similar effects have been identified for Mn in InAs [34,35]. Consequently, the symmetry decreases as the impurities approach closer to the surface. Similar depth dependence is observed for Fe impurities. The low Fe concentration achieved in each sample did not allow for a systematic study of Fe impurities at different depths. Nonetheless, a qualitatively similar depth dependence to Mn is observed for Fe, even if each impurity could not be unambiguously attributed to a specific depth. We estimate the

Fe dopant shown in Fig. 2 to be two or three monolayers below the surface.

The Fe atoms in the first monolayers exhibit a higher degree of symmetry with respect to the  $[1\bar{1}0]$  direction than is seen for Mn atoms. The higher binding energy and weaker hybridization expected for Fe states with the host crystal explains this difference. In addition, the surface, as well as the strain it produces, does not affect the wave functions of these Fe states significantly as they are more localized. Studies of the dependence of the wave-function symmetry on acceptor binding energy indicate that the deeper the acceptor level the more symmetric it appears [36]. The deep acceptor states of Fe are thus expected to possess a stronger impurity character than the Mn acceptor states.

In the STM experiment, at positive bias voltages, electrons are injected in the empty states of the semiconductor sample, that is, into the conduction band and the empty energy levels associated with Fe impurities. Under these conditions, the semiconductor's bands bend upwards due to tip-induced band bending (TIBB) [20,37]. The Fermi level in the bulk is in the gap, close to the top of the valence band; therefore, the deep  $e$  and  $t_2$  levels, located 510 and 880 meV above the valence band edge, respectively, are empty. The majority-spin  $t_2$  level is occupied. Thus, the energy level occupation of Fig. 1(b), which corresponds to the electronic configuration of the  $\text{Fe}^{3+}$  isoelectronic acceptor state, applies. This implies that electrons tunneling through the deep  $e$  and  $t_2$  levels are responsible for the bright electronic contrast observed in the empty-states images. The anisotropic shape is attributed solely to the  $t_2$  core level wave function, as the  $e$  level is expected to have a much more localized contrast. Comparing STM height profiles taken across the neutral Mn and Fe impurities shows that, in the case of Fe, the enhancement of the local density of states (LDOS) is more localized on the impurity itself. This is consistent with the deep nature of the  $\text{Fe}^{3+}$  isoelectronic acceptors levels, as well as the additional and localized tunneling channel due to the presence of an  $e$  state in the band gap for Fe. This explains why only Fe atoms a few monolayers from the surface can be resolved.

The validity of the analysis above is supported by further experimental and theoretical investigations. A spatially resolved I-V spectroscopy experiment at 5 K was performed to study a single subsurface Fe impurity. The data acquisition was set such that the tip-sample distance was the same for every point. This is achieved by moving the tip with the feedback loop on at a voltage at which the topography is uniform across the whole image (here  $V = +2.5$  V). At each point, I-V curves were taken after the tip had been brought closer to the surface by 0.2–0.5 nm with the feedback loop off. These settings are chosen to avoid any topography cross talk in the spatially-resolved I-V spectroscopy data.

A 7.5-nm-wide current profile taken across the subsurface Fe impurity along the  $[001]$  direction is shown in Fig. 2(b) for voltages between 0 and 1.6 V. This plot shows two distinct onsets around +0.45 V and +1.0 V, which are attributed to  $e$  and  $t_2$  acceptor states related to Fe, while the onset of the conduction band is visible at a voltage of 1.55 V. The fact that the current signal does not drop directly to zero at energies above these two onsets is attributed to the tunneling from states below the Fermi energy in the tip. In this paper we have chosen to show current profiles instead of often-used  $dI(x, V)/dV$

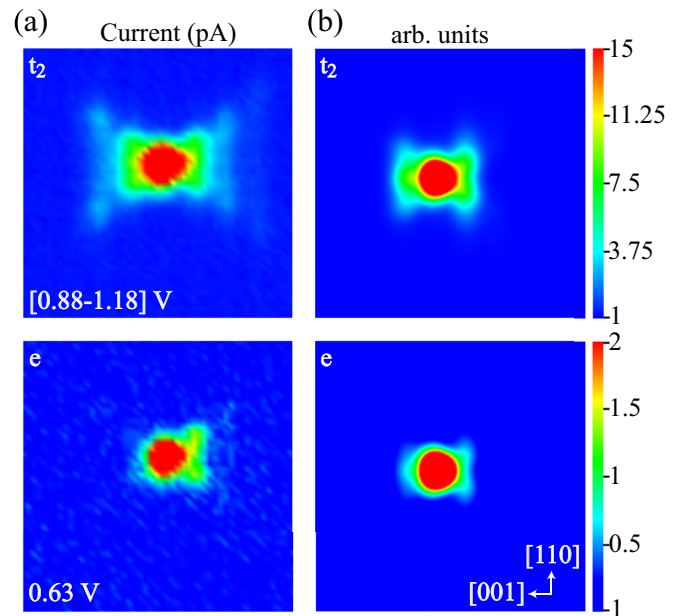


FIG. 3. (a)  $6.5 \times 6.5$ -nm experimental current ( $I$ ) maps averaged in a bias window  $[0.88\text{--}1.18]$  V (top) and taken at 0.63 V (bottom) on a single Fe impurity at 5 K. The spatial extent of these states is consistent with those expected for the deep Fe states of  $t_2$  symmetry (higher energy) and  $e$  (lower energy). (b)  $6.5 \times 6.5$ -nm plots of the calculated spin-averaged real-space probability density of the  $d$  states of  $t_2$  (top) and  $e$  (bottom) symmetry, two atomic planes away from a single Fe impurity. The calculation has been spatially broadened at each atomic position by a normalized Gaussian with a 0.25-nm width.

profiles due to the lower noise associated with the current profiles. As can be seen in the Supplemental Material [32], where we show the corresponding  $dI(x, V)/dV$  profiles, our interpretations of the measurements are not affected by this choice.

### III. COMPARISON WITH TIGHT-BINDING CALCULATIONS OF Fe IMPURITY STATES

The spatial structure of these features can be most clearly seen by considering the  $I(x, y)$  maps taken at 0.63 V and coming from the  $[0.88\text{--}1.18]$ -V bias window. The current map of the  $t_2$  state is averaged over a current window in order to reduce the noise level, which is larger than the noise level at the  $e$ -state energy. The corresponding  $dI(x, V)/dV$  maps are included in the Supplemental Material [32]. The selected energy positions are chosen to show the largest contributions to each peak. These are presented in Fig. 3(a) in the bottom and top panels, respectively. The spatial extent of these two states is clearly different. The lower-energy state is strongly localized on the Fe impurity itself. The wave function of this state is almost isotropic and extends over  $\sim 0.75$  nm. Two small features can be seen extending in the  $[00\bar{1}]$  direction. The higher localization of this state is explained by the weak hybridization of the  $e$  states with states of the host crystal, due to an incompatibility of  $e$ -like  $d$  orbitals with host  $p$  orbitals [Fig. 1(a)]. The higher energy state presents extensions into the host semiconductor in a crosslike shape. The wave function of

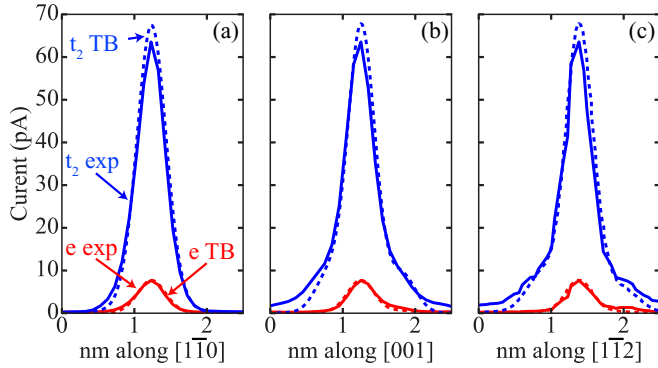


FIG. 4. Current measured (solid lines) and calculated (dashed lines) near a single Fe impurity at 5 K; at 0.63 V for the  $e$  state (in red) and averaged in a bias window [0.88–1.118] V for the  $t_2$  state (in blue) along the (a) [001], (b) [110], and (c) [112] directions, taken two layers away from the Fe impurity. The same broadening as Fig. 3 is used.

this state is anisotropic and extends over  $\sim 2.5$  nm along the [001] direction and 2 nm along the [110] direction.

These features are well reproduced by a tight-binding calculation, shown in Fig. 3(b). We calculate the Green's functions for bulk GaAs using an  $sp^3$  tight-binding description [26]. The effect of the impurity is evaluated using a Koster-Slater technique [38] similar to that used to determine the acceptor-state wave function for Mn in GaAs [27]. Here  $d$  orbitals are added to the Fe impurity site in the calculations, and the  $d$ -orbital energies and hopping matrix elements are introduced. The  $d$ -orbital energies are determined from experimental measurements of the Fe midgap states [29,30]. The on-site nonmagnetic potential for  $e$  states is  $-31.15$  eV and for  $t_2$  states is  $-30.49$  eV. The on-site magnetic potential for  $e$  states is  $-2$  eV and for  $t_2$  states is  $-1$  eV. As the  $d$  orbitals on the Fe are  $3d$ , whereas those included in tight-binding descriptions of GaAs [39] are  $4d$ , the  $pd$  hopping parameters must be determined separately. The  $pd\sigma$  hopping between Fe  $3d$  and As  $4d$  should be much smaller than that between Ga and As  $4d$  states, and the optimal value we determine,  $-0.0712$  eV, is less than one-tenth of that ( $-1.78$  eV) parametrized for  $pd\sigma$  hopping in GaAs [39]. Once the extent of the  $t_2$  state is set, the extent of the  $e$  state is determined from a very small

$pd\pi$  contribution; the best fit (0.018 eV) is two orders of magnitude smaller than 1.78 eV, the  $pd\pi$  hopping parameter of GaAs [39]. This very small parameter supports the symmetry arguments of Fig. 1(a).

Figure 3(b) presents the calculated real-space probability density of the  $d$  states of  $t_2$  (top) and  $e$  (bottom) symmetry taken for a cut through the bulk GaAs crystal two layers away from the Fe ion. The shapes of the calculated LDOS are in agreement with the experimental wave functions and the calculated LDOS is concentrated heavily on the impurity itself. The latter result is consistent with the experimental STM height profile taken above single Fe impurities. Agreement is also evident in Fig. 4 for line cuts along three directions.

#### IV. CONCLUDING REMARKS

The features observed here differ greatly from those measured for Fe in the surface layer [24,25]. For Fe in the surface layer the two peaks found at 0.88 and 1.5 eV were interpreted as corresponding to splitting of the  $t_2$  states due to symmetry breaking at the surface. Their results are supported by the odd and even spatial symmetry, as well as similar spatial extent, of the two states appearing in the differential conductance maps at the corresponding energies [24]. Impurity states at the surface [40,41] are known to be quite different from those even a layer below the surface, which are much less sensitive to the influence of the surface [42,43]. The two states in our Figs. 3 and 4 do not exhibit the even and odd symmetry expected for states resulting from a splitting of the  $t_2$  state by the effect of the reconstructed surface. Instead, the shape and the spatial extent of these states are consistent with that expected, and calculated theoretically, if the  $t_2$  states are not split.

#### ACKNOWLEDGMENTS

We acknowledge support from the European Community's Seventh Framework Programme (Grant No. PF7/2007-2013) SemiSpinNet (experiment), an AFOSR MURI (theoretical analysis), and the US Department of Energy, Office of Basic Sciences, Division of Materials Science and Engineering under Award DE-SC0016447 (computation). J.B. and V.R.K. contributed equally to this work.

- 
- [1] P. M. Koenraad and M. E. Flatté, *Nat. Mater.* **10**, 91 (2011).
  - [2] M. Steger, K. Saeedi, M. L. W. Thewalt, J. J. L. Morton, H. Riemann, N. V. Abrosimov, P. Becker, and H.-J. Pohl, *Science* **336**, 1280 (2012).
  - [3] F. Jelezko and J. Wrachtrup, *Phys. Status Solidi A* **203**, 3207 (2006).
  - [4] G. Balasubramanian, P. Neumann, D. Twitchen, M. Markham, R. Kolesov, N. Mizuochi, J. Isoya, J. Achard, J. Beck, J. Tissler, V. Jacques, P. R. Hemmer, F. Jelezko, and J. Wrachtrup, *Nat. Mater.* **8**, 383 (2009).
  - [5] J. Bocquel, V. R. Kortan, C. Şahin, R. P. Champion, B. L. Gallagher, M. E. Flatté, and P. M. Koenraad, *Phys. Rev. B* **87**, 075421 (2013).
  - [6] F. A. Zwanenburg, A. S. Dzurak, A. Morello, M. Y. Simmons, L. C. L. Hollenberg, G. Klimeck, S. Rogge, S. N. Coppersmith, and M. A. Eriksson, *Rev. Mod. Phys.* **85**, 961 (2013).
  - [7] A. M. Yakunin, A. Y. Silov, P. M. Koenraad, J.-M. Tang, M. E. Flatté, J.-L. Primus, W. Van Roy, J. De Boeck, A. M. Monakhov, K. S. Romanov, I. E. Panaiotti, and N. S. Averkiev, *Nat. Mater.* **6**, 512 (2007).
  - [8] M. W. Doherty, F. Dolde, H. Fedder, F. Jelezko, J. Wrachtrup, N. B. Manson, and L. C. L. Hollenberg, *Phys. Rev. B* **85**, 205203 (2012).
  - [9] J.-M. Tang, J. Levy, and M. E. Flatté, *Phys. Rev. Lett.* **97**, 106803 (2006).

- [10] T. Chanier, C. Pryor, and M. E. Flatté, *Phys. Rev. B* **86**, 085203 (2012).
- [11] J.-M. Tang and M. E. Flatté, *Phys. Rev. B* **72**, 161315(R) (2005).
- [12] T. O. Strandberg, C. M. Canali, and A. H. MacDonald, *Phys. Rev. Lett.* **106**, 017202 (2011).
- [13] K. A. Kikoin and V. N. Fleurov, *Transition Metal Impurities in Semiconductors* (World Scientific, New York, 1994).
- [14] M. D. McCluskey and E. E. Haller, *Dopants and Defects* (CRC Press, New York, 2012).
- [15] H. P. Hjalmarson, P. Vogl, D. J. Wolford, and J. D. Dow, *Phys. Rev. Lett.* **44**, 810 (1980).
- [16] P. Vogl and J. M. Baranowski, *Acta Phys. Polo.* **A67**, 133 (1985).
- [17] Z. F. Zheng, M. B. Salmeron, and E. R. Weber, *Appl. Phys. Lett.* **64**, 1836 (1994).
- [18] Z. F. Zheng, M. B. Salmeron, and E. R. Weber, *Appl. Phys. Lett.* **65**, 790 (1994).
- [19] R. de Kort, M. C. M. M. van der Wielen, A. J. A. van Roij, W. Kets, and H. van Kempen, *Phys. Rev. B* **63**, 125336 (2001).
- [20] A. M. Yakunin, A. Y. Silov, P. M. Koenraad, J. H. Wolter, W. Van Roy, J. De Boeck, J.-M. Tang, and M. E. Flatté, *Phys. Rev. Lett.* **92**, 216806 (2004).
- [21] G. Mahieu, B. Grandidier, D. Deresmes, J. P. Nys, D. Stiévenard, and P. Ebert, *Phys. Rev. Lett.* **94**, 026407 (2005).
- [22] D. Kitchen, A. Richardella, J.-M. Tang, M. E. Flatté, and A. Yazdani, *Nature (London)* **442**, 436 (2006).
- [23] J.-M. Jancu, J.-C. Girard, M. O. Nestoklon, A. Lemaître, F. Glas, Z. Z. Wang, and P. Voisin, *Phys. Rev. Lett.* **101**, 196801 (2008).
- [24] A. Richardella, D. Kitchen, and A. Yazdani, *Phys. Rev. B* **80**, 045318 (2009).
- [25] S. Mühlenberend, M. Gruyters, and R. Berndt, *Phys. Rev. B* **88**, 115301 (2013).
- [26] D. J. Chadi, *Phys. Rev. B* **16**, 790 (1977).
- [27] J.-M. Tang and M. E. Flatté, *Phys. Rev. Lett.* **92**, 047201 (2004).
- [28] M. R. Mahani, M. F. Islam, A. Pertsova, and C. M. Canali, *Phys. Rev. B* **89**, 165408 (2014).
- [29] E. Malguth, A. Hoffmann, and M. R. Phillips, *Phys. Status Solidi B* **245**, 455 (2008).
- [30] K. Pressel, A. Dornen, G. Ruckert, and K. Thonke, *Phys. Rev. B* **47**, 16267 (1993).
- [31] S. Loth, M. Wenderoth, L. Winking, R. G. Ulbrich, S. Malzer, and G. H. Döhler, *Phys. Rev. Lett.* **96**, 066403 (2006).
- [32] See Supplemental Material at <http://link.aps.org/supplemental/10.1103/PhysRevB.96.075207> for the apparent difference in STM measurements between Fe and C dopants, and showing the  $dI/dV$  plots corresponding to Fig. 3.
- [33] C. Çelebi, J. K. Garleff, A. Y. Silov, A. M. Yakunin, P. M. Koenraad, W. Van Roy, J.-M. Tang, and M. E. Flatté, *Phys. Rev. Lett.* **104**, 086404 (2010).
- [34] F. Marczinowski, J. Wiebe, J.-M. Tang, M. E. Flatté, F. Meier, M. Morgenstern, and R. Wiesendanger, *Phys. Rev. Lett.* **99**, 157202 (2007).
- [35] S. Loth, M. Wenderoth, and R. G. Ulbrich, *Phys. Rev. B* **77**, 115344 (2008).
- [36] C. Çelebi, P. M. Koenraad, A. Y. Silov, W. Van Roy, A. M. Monakhov, J.-M. Tang, and M. E. Flatté, *Phys. Rev. B* **77**, 075328 (2008).
- [37] R. M. Feenstra, G. Meyer, F. Moresco, and K. H. Rieder, *Phys. Rev. B* **66**, 165204 (2002).
- [38] G. F. Koster and J. C. Slater, *Phys. Rev.* **95**, 1167 (1954).
- [39] J.-M. Jancu, R. Scholz, F. Beltram, and F. Bassani, *Phys. Rev. B* **57**, 6493 (1998).
- [40] D. Lee and J. Gupta, *Nano Lett.* **11**, 2004 (2011).
- [41] J. Garleff, A. Wijnheijmer, C. N. v. d. Eenden, and P. Koenraad, *Phys. Rev. B* **84**, 075459 (2011).
- [42] J. K. Garleff, C. Çelebi, W. Van Roy, J.-M. Tang, M. E. Flatté, and P. M. Koenraad, *Phys. Rev. B* **78**, 075313 (2008).
- [43] J. K. Garleff, A. P. Wijnheijmer, A. Y. Silov, J. van Bree, W. Van Roy, J.-M. Tang, M. E. Flatté, and P. M. Koenraad, *Phys. Rev. B* **82**, 035303 (2010).